Topological plasmonically induced transparency in a graphene waveguide system

Di Zhang,[1] Shengxuan Xia,[1,2,*] Wei Xu,[1] Xiang Zhai,[1] and Lingling Wang[1]

[1] *Key Laboratory for Micro/Nano Optoelectronic Devices of Ministry of Education & Hunan Provincial Key Laboratory of Low-Dimensional Structural Physics and Devices, School of Physics and Electronics, Hunan University, Changsha 410082, China*

[2] *State Key Laboratory of Millimeter Waves, Southeast University, Nanjing 210096, China*

(Received 24 January 2024; revised 8 May 2024; accepted 4 June 2024; published 17 June 2024; corrected 12 February 2025)

Plasmonically induced transparency (PIT) is a physical phenomenon that mimes electromagnetically induced transparency in plasmonic systems. However, it is challenging to maintain its line shape with the presence of disorders or defects, mainly because it is highly susceptible to structural parameters. Herein, a two-dimensional graphene plasmonic system, which is composed of a few periods of vertically arranged graphene-nanoribbon (GNR) pairs coupled with a graphene waveguide, is proposed. By constructing GNRs to form bright and dark plasmon modes with topologically nontrivial phases, the optical response of the graphene waveguide system gives rise to robust PIT effects that exhibit an immunity to a certain degree of various parametric perturbations and imperfections. A three-level plasmonic system is demonstrated to explain the formation mechanism of the PIT effects, and the corresponding results agree well with the numerical ones. Combining topology with PIT helps to reduce the impact of parametric disorders and defects, which benefits the PIT devices with design freedom and higher stability.

DOI: 10.1103/PhysRevB.109.245420

I. INTRODUCTION

Surface plasmons are electromagnetic oscillations formed by coupling incident light to free electrons, which greatly facilitates the interaction between light and matter owing to their ability to support optical modes in deep subwavelength scale and overcome the classical diffraction limit [1–4]. During the past decades, surface plasmons have been investigated extensively due to their promising applications in diverse fields, including optical modulators [5], nanolasers [6], sensors [7], and particle manipulation [8,9]. In addition, this optical phenomenon also provides a feasible platform to achieve electromagnetically induced transparency (EIT) in plasmonic systems.

A plasmon mode can be either bright (superradiant) or dark (subradiant) depending on whether the coupling strength between an external incident light and the plasmonic mode is strong or weak [10–12]. The bright mode has a smaller quality factor as it can couple strongly with light, while the dark mode cannot directly (or can weakly) couple to the light but can indirectly couple through the bright mode, thus exhibiting a significantly larger quality factor. Therefore, there are two excitation paths for the bright mode, and their destructive interferences form a narrow transparency window inside the original wide absorption band of the bright mode, inducing an interesting phenomenon called *plasmonically induced transparency* (PIT) [13–16]. The transparency window is associated with a strong dispersion and can lead to a dramatic reduction of group velocity, which enables propagating light to slow down and further unlocks many practical applications, such as slow-light devices [17], highly sensitive sensors [18], and bandpass plasmonic filters [19]. Various plasmonic structures have been proposed to realize the PIT effect, e.g., metallic metamaterials [20,21], graphene metasurfaces [22,23], and plasmonic waveguide [24]. Unfortunately, the traditional PIT phenomenon suffers from low ability to tolerate geometrical disorders and defects since its line shape strongly depends on the position of the bright and dark modes.

The concept of topology has recently expanded from condensed matter theory to classical wave systems. Among them, topological photonics has attracted much attention because it enables the emergence of optical phenomena and offers a method to realize the unidirectional and robust transportation of light waves [25–31]. So far, the concept of topology has been successfully applied to realize topologically protected Fano resonance in acoustic [27] and optical [32] systems. Although several approaches have been proposed to realize topologically protected EIT in cavity-coupled waveguide systems based on photonic crystals [25,26,28], the topologically protected PIT effect has been elusive. Considering that the emergence of the PIT effect as well as the line shape and width of the transparency window strongly depend on the coupling strength/resonant frequencies between/of the bright and dark modes, the change of relative positions of the resonators strongly tunes and even destroys the transparency window, greatly hindering tailored nanophotonic applications and on-chip integration of PIT-based devices.

In this paper, we extend the concept of topology to a graphene-based plasmonic system that supports the PIT effect to overcome this shortcoming. As a proof-of-principle example, we use multilayer graphene nanoribbons (GNRs) with nontrivial topological phases to construct topological bright and dark plasmon modes, which further couple with a graphene waveguide to build a three-level plasmonic system. We will show how this system permits the existence of the

*Contact author: shengxuanxia@hnu.edu.cn

 ©2024 American Physical Society

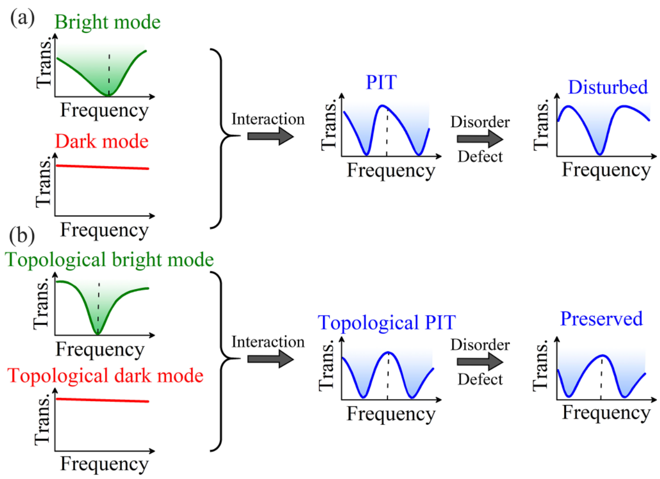

FIG. 1. Schematic of the proposed topological plasmonically induced transparency (PIT) effect. (a) The line shape of conventional bright- and dark-mode-induced PIT effects may be seriously damaged by a certain level of disorders or defects, while (b) topological bright- and dark-mode-resulted topological PIT effect shows robustness to the same disorders and defects.

topological PIT effect and how the PIT effect responds to structural imperfections, such as disorders and defects for various parameters. Meanwhile, the coupled mode theory is demonstrated to explain the formation mechanism of PIT, and the analytical results are found to be in good agreement with the numerical simulations.

II. RESULTS AND DISCUSSIONS

A. Topological concept and model

Figure 1 schematically shows the realization of the proposed concept of the topological PIT effect. The basic idea of generating the PIT effect can be attributed to the constructive and destructive interferences between bright- and dark-mode resonance supported by different plasmonic resonators. The bright mode suffers from radiation losses, resulting in a transmission dip/absorption peak in the spectrum, while the dark mode shows weak or no response in the spectrum. Unfortunately, traditional PIT systems are sensitive to structural perturbations. As a result, the PIT line shape is destroyed with the existence of disorders or defects, as shown in Fig. 1(a). To improve the stability of the PIT window, topological bright and dark modes are constructed to form the topologically protected PIT effect, as displayed in Fig. 1(b). This approach guarantees that the transparent window remains due to the inherent robustness provided by the topologically nontrivial phases, even in the presence of disorders or defects, surpassing what can be achieved through conventional PIT methods.

To this end, we propose using a graphene waveguide coupled with two sets of topological GNRs, as shown in Fig. 2(g),

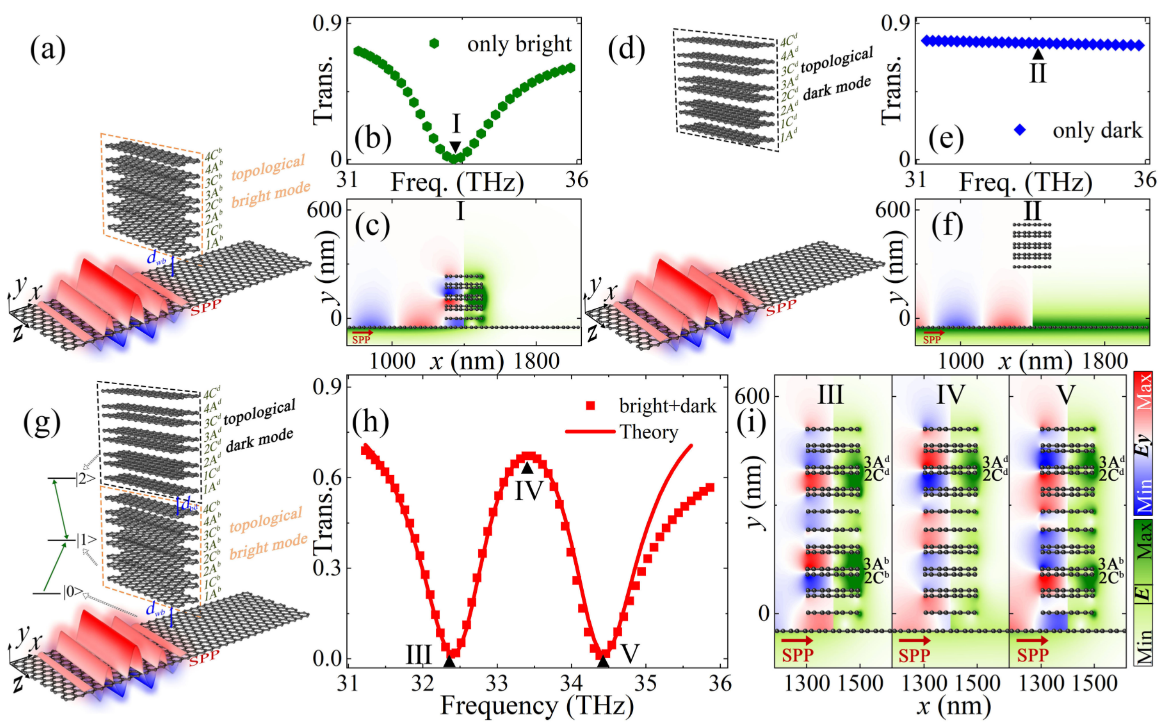

FIG. 2. (a) Schematic diagrams of the plasmonic system with only topological bright mode, (d) only topological dark mode, and (g) both topological bright and dark modes forming the proposed topological plasmonically induced transparency (PIT) system. The orange/black-dashed box shows the bright/dark mode resonator with four Su-Schrieffer-Heeger (SSH) units. Labels XA^i/XC^i refer to the positions of the sublattice A/C in the Xth unit in the bright ($i = b$) and dark ($i = d$) mode resonators. (b) Transmission spectrum for the cases with only topological bright mode; the full range of transmission spectrum is shown in Fig. S2 of the Supplemental Material [38]); (e) only topological dark mode, and (h) both of them forming topological PIT, where the solid line presents theoretical results, while dots are from numerical simulations. (c) Spatial field distributions of $E_y/|E|$ at the positions of I, (f) II, and (i) III–V labeled in (b), (e), and (h), respectively. The fields at I, II, and IV are all located at 33.4 THz. Note that we set $\beta = \frac{5}{6}$ in all cases of this figure.

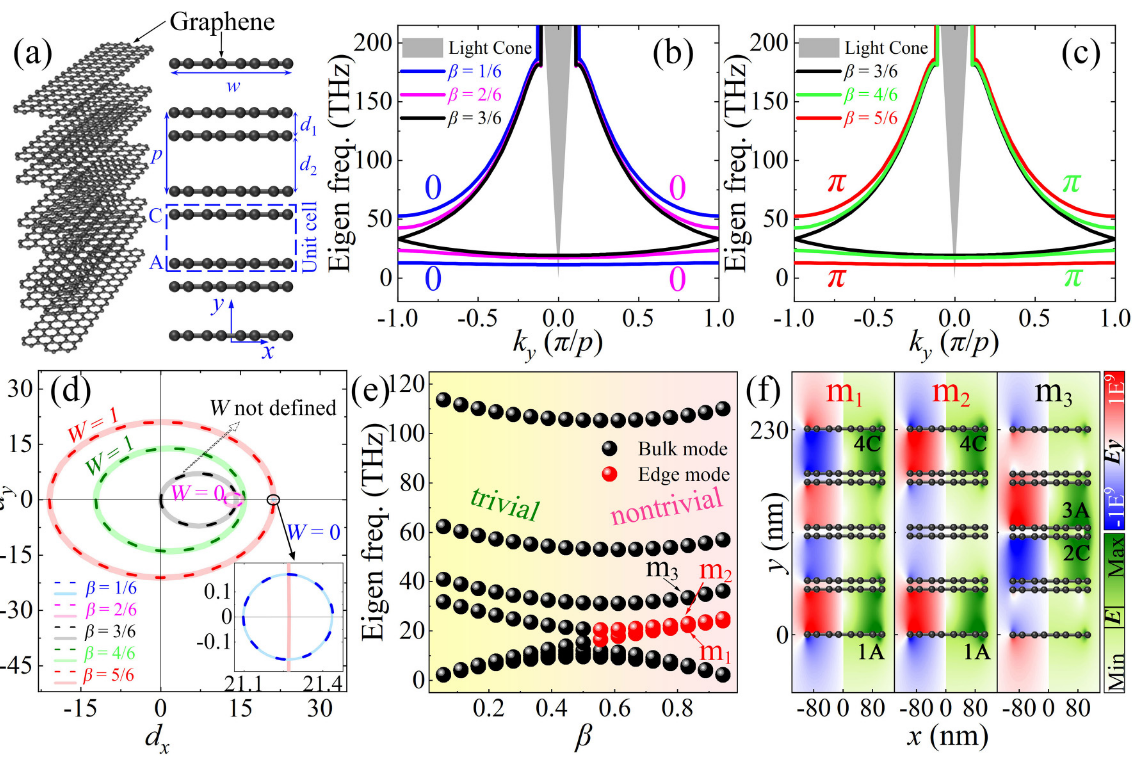

FIG. 3. (a) Schematic diagram of the proposed bright/dark mode resonator with four Su-Schrieffer-Heeger (SSH) units. (b) and (c) The band structures for different β in one SSH unit, with the light cone presented by the gray background area, where the upper energy band becomes anomalous. 0 and π refer to the values of the Zak phase of corresponding bands. (d) The winding vectors in the first Brillouin zone for different β, with the insert shows the zoomed-in case of $\beta = \frac{1}{6}$. The values of W are labeled with the same color as the lines. Note that the winding number of the case with $\beta = 0.5$ is not defined, and the solid and dashed lines correspond to the upper and lower bands, respectively. (e) Eigenmode spectra of four SSH units with varying β. (f) Spatial field distributions of $E_y/|E|$ for the topological bulk state (m_3) and two degenerate topological edge states (m_1 and m_2) for $\beta = \frac{5}{6}$.

to realize topological PIT effects. The topological system is analogous to the one-dimensional Su-Schrieffer-Heeger (SSH) model, comprising stacked GNRs arranged with alternating spacing in the y direction. We propose constructing two topological resonators that are built by stacking four units of the SSH model, with each unit hosting two ribbon sublattices labeled A and C, as shown in Figs. 3(a) and 2(g), respectively. The width of the GNRs is set as $w = 200$ nm, and the distances within and between the SSH units in the vertical direction are set as d_1 and d_2, which builds a structure with a period of $p = d_1 + d_2 = 60$ nm. The distance between the lower resonator and the graphene waveguide is set as d_{wb}, while the spacing between the two stacked resonators is denoted by d_{bd}, and they are fixed as $d_{wb} = d_{bd} = 50$ nm, unless otherwise specified. Note that the geometrical parameters used here are chosen for conceptual demonstration; our conclusions are general and do not depend on the choice of the parameters. In addition, the proposed PIT device with graphene multilayers and parameters shown above is experimentally feasible with state-of-the-art techniques [33–37]; an alternative method to the actual physical realization is provided in Sec. S4 in the Supplemental Material [38].

To demonstrate our concept, we numerically calculate the optical response of the waveguide system by performing full-wave simulations with the finite-element method (COMSOL Multiphysics). In our simulations, we model graphene as a two-dimensional surface current tangential to the graphene surface as $\mathbf{J}_s = \sigma_g(\omega)\mathbf{E}_{//}$, where $\mathbf{J}_s$ is the surface current, $\mathbf{E}_{//}$ is the in-plane component of the electric field, and $\sigma_g(\omega)$ is the optical conductivity of graphene, which is generated from the Kubo formula and consists of both intraband and interband contributions [39–41]. Detailed parameters and the settings of COMSOL Multiphysics can be found in Secs. S1 and S2 in the Supplemental Material [38].

Before going further, it is necessary to rule out the topological nature of one unit of SSH ribbon pairs. First, we plot the band structure of one unit of the dimerized ribbons in the first Brillouin zone in Figs. 3(b) and 3(c) for different dimerization parameters β, which is defined as $\beta = d_2/p$ for the convenience of describing the topological nature of the structure. These figures show that two bands with distinguishable energy are supported, where the energy bands of the cases with β are the same as those of $1 - \beta$. Additionally, one may find that the band gap between the two bands increases as β approaches 0 and 1. Then the topology of these bands can be physically distinguished by the winding number, which is defined for a deformed Brillouin zone to characterize the topological properties of the proposed SSH model [48,50,51].

To this end, we need to consider the plasmon modes supported by the GNRs and their couplings. Previous works have revealed that plasmonic couplings are dominated by first-order dipole excitation, while the other high-order mode contributions can be safely neglected [14]. If each dipole mode in the sublattice A or C corresponds to a bosonic excitation with a resonance frequency ω_0, the plasmonic couplings among them lead to the formation of collective modes throughout the ribbon layers [48]. Based on that, the collective dipolar modes mimic the band structure of the SSH Hamiltonian as [48]

$$H = \begin{pmatrix} \omega_0 & Cg \\ Cg^* & \omega_0 \end{pmatrix}, \tag{1}$$

where C is the coupling constant that is expressed as $C = \omega_0 a^3/p^3 2$, with a being a length scale that relates to the strength of the dipolar mode excitations, g is the intersublattice function that reflects the intra- and interunit-cell couplings between the near ribbons and reads

$$g = \left(\frac{p}{d_2}\right)^3 + \left(\frac{p}{d_1}\right)^3 \exp(-ik_y p), \tag{2}$$

with k_y being the y component of wave vector. Therefore, the SSH dispersion shown in Figs. 3(b) and 3(c) can be calculated by the Hamiltonian shown in Eq. (1):

$$\omega_\pm = \omega_0 \pm C|g|, \tag{3}$$

where the $\pm$ symbols refer to the upper/lower energy band.

In this sense, the winding numbers of the two-band system can be decomposed into $\mathbf{H} = \boldsymbol{\sigma}\cdot\mathbf{d}$, with $\boldsymbol{\sigma} = (\sigma_x, \sigma_y)$ being the Pauli vector, and

$$\mathbf{d} = (d_x, d_y) = C|g|(\cos\phi, -\sin\phi) \tag{4}$$

being the k-dependent winding vector, with ϕ being defined as $e^{i\phi} = g/|g|$ [48]. As the wave vector runs through the first Brillouin zone (that is, k_y goes from 0 to 2π), its two components outline a closed Wilson loop in the $d_x - d_y$ plane due to the periodicity of the bulk momentum-space Hamiltonian [48]. The topology of this loop is then characterized by an integer called bulk winding number W, which counts the number of times the loop winds around the origin of the $d_x - d_y$ plane. That is, if this loop encloses the origin n times, the value of W takes n, which corresponds to a Zak phase θ_Z of $n\pi$ and the presence ($n \neq 0$) (absence, $n = 0$) of the topological state [52]. For example, for the cases with $\beta = \frac{5}{6}$ ($\frac{1}{6}$) in Fig. 3(c) [Fig. 3(b)], we have $W = 1$ (0) [or correspondingly the Zak phase of π (0)] since the loop encloses the origin for one (zero) time, while for the case with $\beta = \frac{3}{6}$, the winding number is not defined, as shown in Fig. 3(d). At this stage, our results have demonstrated a generic principle to identify the topological nature of the ribbon pairs through the value of Zak phase, that is, we have $\theta_z = \pi$ (0) when $\beta > \frac{1}{2}$ ($< \frac{1}{2}$), corresponding to the topologically nontrivial (trivial) phase of the resonator and with a topological phase transition at $\beta = 0.5$.

The proposed concept to realize topological PIT effects is based on strong coupling between two topological resonators; therefore, it is essential to analyze the topological nature of the bright and dark mode resonators. Figure 3(e) depicts the eigenmode distributions crossing a range of β with four SSH units (eight GNRs). For the topologically trivial phase, the field of all plasmon modes is distributed either in a few or across the entire ribbons, which are referred to as bulk states. Because the topological phase of the case with $\beta > 0.5$ is nontrivial, all the plasmon modes are topologically protected in this case. Therefore, for the topologically nontrivial phase, two notable topological states within the midgap of the energy band appear and degenerate as β increases. These two modes always exist if $\beta > 0.5$ and are featured by their field highly localized in the topmost and bottommost ribbon layers and, thus, are called topological edge states, as shown by m_1 and m_2 in Fig. 3(f). A topological bulk state donated as m_3 is also shown for comparison, with its fields highly localized within the sublattices 2C and 3A.

B. Realization of topological PIT

Now we start to explore how to use topological modes to achieve PIT effects, as shown in Fig. 2(g), by using a graphene waveguide to directly and indirectly couple with two stacked topological resonators. Before going further, it is important to explore the optical property of the case with only one topological resonator and how its interaction with the waveguide modulates the output transmission. Figure 2(a) sketches the structure with a graphene waveguide coupled with only the topological bright-mode resonator. The corresponding transmission spectrum is plotted in Fig. 2(b), which clearly depicts a transmission dip near zero at 33.4 THz. To uncover the reason causing this dip, we illustrate the plasmon field distributions in Fig. 2(c). This figure clearly displays that a topological bulk mode with fields highly concentrated in the sublattices 2C and 3A [the mode corresponding to m_3 in Fig. 3(f)] is excited and so strongly couples with the graphene waveguide that the transmission coefficient of the structure then reduces to zero. In other words, when the plasmon resonator is close enough to the graphene waveguide, e.g., 50 nm we used here, it can directly and strongly couple with the bus waveguide, forming the mode we called the *topological bright mode* since its topological phase is nontrivial.

As the distance between the resonator and the bus waveguide increases, the transmission dip gradually increases. When it is far from the bus waveguide, e.g., increasing to 330 nm, as shown in Fig. 2(d), no transmission dip appears [see Fig. 2(e), like the case with only the bus waveguide], and therefore, no plasmon mode is excited in the resonator [see Fig. 2(f)]. In this case, we call the mode in the resonator the *topological dark mode* since it cannot directly couple with the bus waveguide. In other words, whether a plasmon resonator acts as a bright or a dark mode is determined by whether its distance to the bus waveguide is close enough. More discussions about how this coupling distance affects the output of the system can be found in Sec. S5 of the Supplemental Material [38]. Interestingly, when both the bright- and dark-mode resonators are present [as shown in Fig. 2(g)] and strongly coupled to each other, two new transmission dips emerge, and a transparency window [indicated by labels III and V in Fig. 2(h)] appears near the original dip of the case with bright mode only, leading to the formation of the topological PIT effect. The field distributions reveal the nature of these two dips, with their field resonant in-phase and out-of-phase at the lower and higher frequencies, as labeled by III and V in Fig. 2(i), respectively. Finally, we also discuss the cases without topological features (with $\beta = \frac{1}{6}$ and $\frac{1}{2}$) for comparison, where multi-PIT effects are found to be supported by the

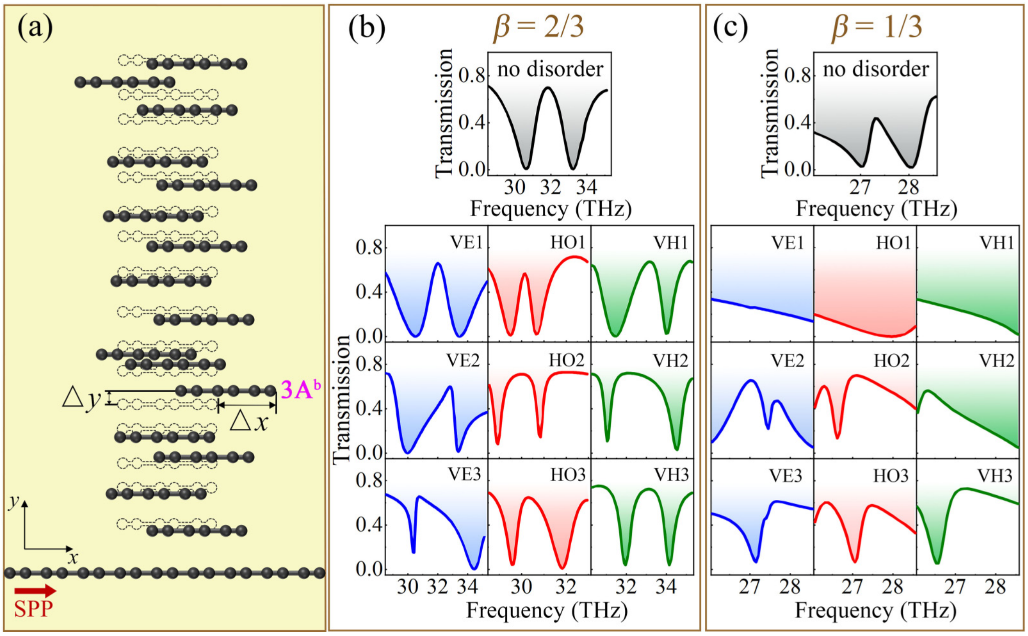

FIG. 4. (a) Schematic of the structure with disorders. The dashed outlines delineate the original positions of graphene nanoribbons (GNRs) with the definition of relative horizontal (Δx) and vertical (Δy) shifts displayed in 3A^b. Transmission spectra of the plasmonically induced transparency (PIT) system with random disorders for the (b) topologically nontrivial ($\beta = \frac{2}{3}$) and (c) trivial ($\beta = \frac{1}{3}$) phases, where the maximum degrees of disorders are chosen as $\Delta x = 30$ nm and $\Delta y = 9$ nm, respectively, and the abbreviations VE, HO, and VH refer to the cases with disorders only in the vertical, horizontal, and an arbitrary direction for convenience, respectively.

bulk modes without the protection of the topology; details are given in Sec. S6 of the Supplemental Material [38].

To further reveal the physical mechanism of the PIT effect, we examine the analogy between our system and the traditional atomic EIT system [see Fig. 2(g)]. According to the theory of the three-level system [53,54], the ground state $|0\rangle$ and the two upper active states $|1\rangle$ and $|2\rangle$ respectively correspond to the bus waveguide, the topological bright mode [labeled by superscripts b in Fig. 2(g)], and the topological dark mode [labeled by superscripts d in Fig. 2(g)]. The direct excitation of the bright mode by the bus waveguide is analogous to the dipole-allowed transition path from $|0\rangle$ to $|1\rangle$. Meanwhile, the indirect excitation of the topological bright mode refers to the transition path connected to the topological dark mode as $|0\rangle$–$|1\rangle$–$|2\rangle$–$|1\rangle$. The two possible pathways interfere destructively, reducing losses and enhancing transmittance. Accordingly, the bright mode can be expressed as $|1\rangle = B(w)e^{i\omega t}$, which strongly couples with the ground bus waveguide $|0\rangle = E_0 e^{i\omega t}$ and the dark mode $|2\rangle = D(w)e^{i\omega t}$. Considering that the eigenfrequencies ω_0 of the topological bright and dark modes are the same, it is reasonable to assume that the damping factors γ_i (where $i = b$ and d refer to the bright and dark modes, respectively) of the two modes satisfy the following relation $\gamma_d \ll \gamma_b \ll \omega_0$. Therefore, the field amplitude of both states can be described by the coupled Lorentz oscillator model as [10,11,15]

$$\begin{pmatrix} \omega - \omega_0 + i\gamma_b & \kappa \\ \kappa & \omega - \omega_0 + i\gamma_d \end{pmatrix} \begin{pmatrix} B \\ D \end{pmatrix} = -\begin{pmatrix} gE_0 \\ 0 \end{pmatrix}. \quad (5)$$

Here, κ is the coupling coefficient between the two topological modes, and g describes the coupling strength between the topological bright mode and the waveguide. The complex amplitude B of the topological bright mode is directly proportional to the polarizability of the PIT system, which can be obtained by

$$B = \frac{-gE_0(\omega - \omega_0 + i\gamma_d)}{(\omega - \omega_0 + i\gamma_b)(\omega - \omega_0 + i\gamma_d) - \kappa^2}. \quad (6)$$

Thus, the transmission of the waveguide can be given as $T = 1 - (B/E_0)^2$. By fitting the simulated data with this equation, we find good agreement between the numerical and theoretical results, as shown by the red dots and solid line in Fig. 2(h).

C. Robustness of topological PIT

One of the most prominent properties that arises due to topology is the protection of the topological modes from disorders and defects, which is absent in traditional systems where the optical response is mainly linked to the resonance in a single resonator. Herein, we first study the stability of the PIT system in the existence of inhomogeneously distributed disorder, which is introduced by shifting the positions of both sublattices A and C randomly in the horizontal and vertical directions within the ranges of $[-\Delta x, \Delta x]$ and $[-\Delta y, \Delta y]$, respectively [see the schematic presentation in Fig. 4(a)]. Although it is impossible to conclude all the cases, we have examined >10 sets of randomly generated data for each range of disorders to validate our proposal and plotted three selected results in Fig. 4(b) with $\beta = \frac{2}{3}$. The case of $\beta = \frac{1}{3}$ is also shown in Fig. 4(c) with the same set of disorders used in Fig. 4(b) for comparison. One may find the salient feature of these transmission spectra: The obvious PIT

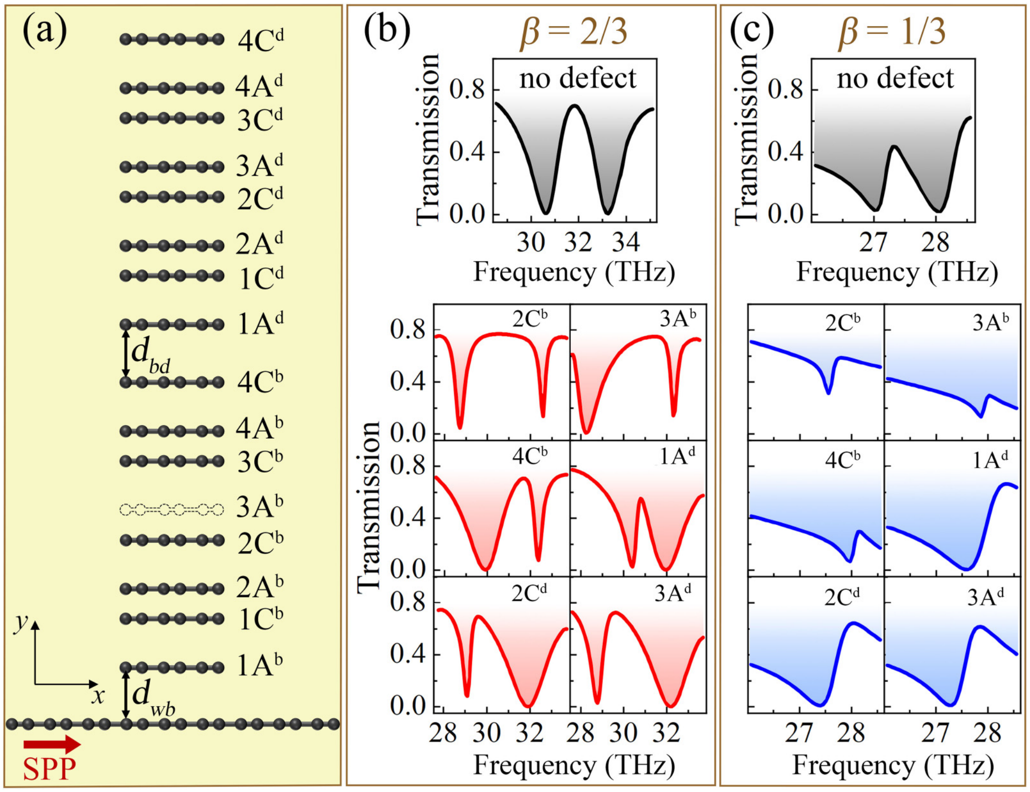

FIG. 5. (a) Schematic of the structure with a defect in the position of $3A^b$ as an example. Transmission spectra of the plasmonically induced transparency (PIT) system with a defect for the (b) topologically nontrivial ($\beta = \frac{2}{3}$) and (c) trivial ($\beta = \frac{1}{3}$) phases.

window is maintained for all kinds of disorders presenting in only the vertical or horizontal direction and in both directions simultaneously, with the maxima degrees of disorder up to $\Delta x = 30$ nm and $\Delta y = 9$ nm (note that $\Delta y < 10$ nm for $\beta = \frac{2}{3}$). For all cases of disorders considered here, the nontrivial Zak phase is always sustained without inducing any topological transition; the PIT effect is well prevented by topology. However, the PIT effect in the topologically trivial case is deeply affected by the same set of disorders for $\beta = \frac{1}{3}$. This is because the presence of disorders induces new localized plasmon modes that strongly destroy their original bright and dark modes and their interactions. Consequently, the PIT spectrum is severely disrupted as one or both transmission dips disappear or new peaks are introduced. Comparing Figs. 4(b) and 4(c), our proposed topological PIT system is immune to a large degree of disorders, benefitting from the robustness to fabrication errors and disorders.

In addition to the stability against disorders, the other feature of the topological PIT effect is its robustness against defects. To examine this, we simulate the performance of the topological PIT system ($\beta = \frac{2}{3}$) under one missing GNR [see Fig. 5(a)] and display the results in Fig. 5(b). We have calculated all 16 cases to reach a general conclusion, finding that the PIT window is always maintained due to the protection of topology. Specifically, we pay particular attention to the cases with the defect located at $2C^b$, $3A^b$, $2C^d$, and $3A^d$ ($4C^b$ and $1A^d$) in Fig. 5(b) since the plasmon fields of the case without a defect strongly localize at these ribbons (they directly affect the coupling strength between the topological bright and dark modes). The PIT window becomes broader or narrower with the existence of the newly introduced defect, but the PIT line shape is preserved quite well by the topology, while for the topologically trivial case with $\beta = \frac{1}{3}$ shown in Fig. 5(c), the absence of one GNR strongly affects the transmission spectrum, and as a result, the PIT line shape is severely destroyed or even disappears.

Finally, we also discuss the topological PIT effect against other parametric perturbations and imperfections to examine the generality of the robustness and compare its performance with topological trivial and conventional PITs. Although, it is impossible to consider all possible cases of parametric perturbations, for the ones considered in Sec. S7 and Table S1 in the Supplemental Material [38] (such as the ribbon position and width, Fermi level, defect, surrounding refractive index, and their combinations under certain degrees), the PIT spectra of the topological nontrivial cases always maintain a prominent PIT window, while for the other two cases without topological features, the spectra are strongly affected by the perturbations, resulting in the disappearance of the PIT effect.

III. CONCLUSIONS

In summary, we have introduced, theoretically explained, and numerically demonstrated the concept of the topological PIT effect. We have designed an SSH model-based GNR array with topologically nontrivial phase to form bright and dark plasmon mode resonators, of which the direct and indirect couplings with a graphene waveguide lead to the topological PIT. In contrast to topological trivial and conventional PIT systems, the proposed topological PIT exhibits superior robustness against various perturbations and imperfections of single and combined parameters, which provides a pivotal advantage of the topological PIT system with an immunity to a certain degree of structural disorders and defects and is desirable for practical fabrication of PIT devices.

ACKNOWLEDGMENTS

This paper was supported by the Natural Science Foundation of Hunan Province, China (No. 2020JJ5028), Changsha Municipal Natural Science Foundation (No. kq2402050), the National Natural Science Foundation of China (No. 11904096), the Fundamental Research Funds for the Central Universities and the Open Project of the State Key Laboratory of Millimeter Waves (No. K202424).

[1] W. L. Barnes, A. Dereux, and T. W. Ebbesen, Surface plasmon subwavelength optics, Nature (London) **424**, 824 (2003).
[2] S. Thongrattanasiri and F. J. García de Abajo, Optical field enhancement by strong plasmon interaction in graphene nanostructures, Phys. Rev. Lett. **110**, 187401 (2013).
[3] A. N. Grigorenko, M. Polini, and K. S. Novoselov, Graphene plasmonics, Nat. Photon. **6**, 749 (2012).
[4] T. T. A. Lummen, R. J. Lamb, G. Berruto, T. LaGrange, L. Dal Negro, F. J. García de Abajo, D. McGrouther, B. Barwick, and F. Carbone, Imaging and controlling plasmonic interference fields at buried interfaces, Nat. Commun. **7**, 13156 (2016).
[5] C. Haffner, D. Chelladurai, Y. Fedoryshyn, A. Josten, B. Baeuerle, W. Heni, T. Watanabe, T. Cui, B. Cheng, S. Saha *et al.*, Low-loss plasmon-assisted electro-optic modulator, Nature (London) **556**, 483 (2018).
[6] P.-J. Cheng, Z.-T. Huang, J.-H. Li, B.-T. Chou, Y.-H. Chou, W.-C. Lo, K.-P. Chen, T.-C. Lu, and T.-R. Lin, High-performance plasmonic nanolasers with a nanotrench defect cavity for sensing applications, ACS Photonics **5**, 2638 (2018).
[7] D. Rodrigo, O. Limaj, D. Janner, D. Etezadi, F. J. García de Abajo, V. Pruneri, and H. Altug, Mid-infrared plasmonic biosensing with graphene, Science **349**, 165 (2015).
[8] D. Sikdar and A. A. Kornyshev, Theory of tailorable optical response of two-dimensional arrays of plasmonic nanoparticles at dielectric interfaces, Sci. Rep. **6**, 33712 (2016).
[9] F. Stete, W. Koopman, and M. Bargheer, Signatures of strong coupling on nanoparticles: Revealing absorption anticrossing by tuning the dielectric environment, ACS Photonics **4**, 1669 (2017).
[10] S. Zhang, D. A. Genov, Y. Wang, M. Liu, and X. Zhang, Plasmon-induced transparency in metamaterials, Phys. Rev. Lett. **101**, 047401 (2008).
[11] N. Liu, L. Langguth, T. Weiss, J. Kastel, M. Fleischhauer, T. Pfau, and H. Giessen, Plasmonic analogue of electromagnetically induced transparency at the Drude damping limit, Nat. Mater. **8**, 758 (2009).
[12] F.-Q. Meng, L. Cao, A. Karalis, H.-T. Gu, M. D. Thomson, and H. G. Roskos, Strong coupling of plasmonic bright and dark modes with two eigenmodes of a photonic crystal cavity, Opt. Express **31**, 39624 (2023).
[13] J. Gu, R. Singh, X. Liu, X. Zhang, Y. Ma, S. Zhang, S. A. Maier, Z. Tian, A. K. Azad, H. T. Chen *et al.*, Active control of electromagnetically induced transparency analogue in terahertz metamaterials, Nat. Commun. **3**, 1151 (2012).
[14] S.-X. Xia, X. Zhai, L.-L. Wang, and S.-C. Wen, Plasmonically induced transparency in double-layered graphene nanoribbons, Photonics Res. **6**, 692 (2018).
[15] H. Cheng, S. Chen, P. Yu, X. Duan, B. Xie, and J. Tian, Dynamically tunable plasmonically induced transparency in periodically patterned graphene nanostrips, Appl. Phys. Lett. **103**, 203112 (2013).
[16] S.-X. Xia, X. Zhai, L.-L. Wang, Y.-J. Xiang, and S.-C. Wen, Plasmonically induced transparency in phase-coupled graphene nanoribbons, Phys. Rev. B **106**, 075401 (2022).
[17] T.-T. Kim, H.-D. Kim, R. Zhao, S. S. Oh, T. Ha, D. S. Chung, Y. H. Lee, B. Min, and S. Zhang, Electrically tunable slow light using graphene metamaterials, ACS Photonics **5**, 1800 (2018).
[18] D. Wu, Y. Liu, L. Yu, Z. Yu, L. Chen, R. Li, R. Ma, C. Liu, J. Zhang, and H. Ye, Plasmonic metamaterial for electromagnetically induced transparency analogue and ultra-high figure of merit sensor, Sci. Rep. **7**, 45210 (2017).
[19] X. Zhong, S. G. Rodrigo, L. Zhang, P. Samori, C. Genet, L. Martin-Moreno, J. A. Hutchison, and T. W. Ebbesen, Waveguide and plasmonic absorption-induced transparency, ACS Nano **10**, 4570 (2016).
[20] D. B. Litt, M. R. Jones, M. Hentschel, Y. Wang, S. Yang, H. D. Ha, X. Zhang, and A. P. Alivisatos, Hybrid lithographic and DNA-directed assembly of a configurable plasmonic metamaterial that exhibits electromagnetically induced transparency, Nano Lett. **18**, 859 (2018).
[21] P. Tassin, L. Zhang, R. Zhao, A. Jain, T. Koschny, and C. M. Soukoulis, Electromagnetically induced transparency and absorption in metamaterials: The radiating two-oscillator model and its experimental confirmation, Phys. Rev. Lett. **109**, 187401 (2012).
[22] S.-X. Xia, X. Zhai, L.-L. Wang, and S.-C. Wen, Plasmonically induced transparency in in-plane isotropic and anisotropic 2D materials, Opt. Express **28**, 7980 (2020).
[23] L. Wang, W. Li, and X. Jiang, Tunable control of electromagnetically induced transparency analogue in a compact graphene-based waveguide, Opt. Lett. **40**, 2325 (2015).
[24] C. Wang, X. Jiang, G. Zhao, M. Zhang, C. W. Hsu, B. Peng, A. D. Stone, L. Jiang, and L. Yang, Electromagnetically induced transparency at a chiral exceptional point, Nat. Phys. **16**, 334 (2020).
[25] J. Dong, B. Zou, and Y. Zhang, Theoretical study of transparent peaks in a topological waveguide-cavity coupled system, Appl. Phys. Lett. **119**, 251101 (2021).
[26] J. Xu, X.-F. Zang, X.-D. Zhan, K. Liu, and Y.-M. Zhu, Manipulating electromagnetic waves in a cavity-waveguide system with nontrivial and trivial modes, Opt. Lett. **47**, 5204 (2022).
[27] F. Zangeneh-Nejad and R. Fleury, Topological Fano resonances, Phys. Rev. Lett. **122**, 014301 (2019).

[28] Z.-B. Zhang, B.-X. Ruan, C. Liu, M. Li, E.-D. Gao, X. Chang, S.-X. Huang, and H.-J. Li, Combining sensitivity and robustness: EIT-like characteristic in a 2D topological photonic crystal, Opt. Express **31**, 26314 (2023).
[29] Z. Jiang, M. Rösner, R. E. Groenewald, and S. Haas, Localized plasmons in topological insulators, Phys. Rev. B **101**, 045106 (2020).
[30] X. Yin, J. Jin, M. Soljacic, C. Peng, and B. Zhen, Observation of topologically enabled unidirectional guided resonances, Nature (London) **580**, 467 (2020).
[31] F. Davoodi and N. Talebi, Unidirectional wave propagation in a topological plasmonic ring resonator via a symmetry-broken excitation scheme, ACS Appl. Nano Mater **6**, 20823 (2023).
[32] Z.-D. Zhang, X.-M. Zhang, S.-Y. Yu, M.-H. Lu, and Y.-F. Chen, Tunable topological Fano resonances in graphene-based nanomechanical lattices, Phys. Rev. Appl. **18**, 054029 (2022).
[33] A. Kasry, M. A. Kuroda, G. J. Martyna, G. S. Tulevski, and A. A. Bol, Chemical doping of large-area stacked graphene films for use as transparent, conducting electrodes, ACS Nano **4**, 3839 (2010).
[34] W. Xu and T.-W. Lee, Recent progress in fabrication techniques of graphene nanoribbons, Mater. Horiz. **3**, 186 (2016).
[35] J. Nong, L. Tang, G. Lan, P. Luo, Z. Li, D. Huang, J. Yi, H. Shi, and W. Wei, Enhanced graphene plasmonic mode energy for highly sensitive molecular fingerprint retrieval, Laser Photonics Rev. **15**, 2000300 (2020).
[36] G. Li, V. Semenenko, V. Perebeinos, and P. Q. Liu, Multilayer graphene terahertz plasmonic structures for enhanced frequency tuning range, ACS Photonics **6**, 3180 (2019).
[37] D. Rodrigo, A. Tittl, O. Limaj, F. J. García de Abajo, V. Pruneri, and H. Altug, Double-layer graphene for enhanced tunable infrared plasmonics, Light Sci. Appl. **6**, e16277 (2017).
[38] See Supplemental Material at http://link.aps.org/supplemental/10.1103/PhysRevB.109.245420 for notes on (1) graphene, (2) comsol Multiphysics, (3) the effects of Fermi energy, (4) the experimental feasibility of the proposed device, (5) the coupling mechanism, (6) the device without the topological features extension, and (7) evidence of robustness, which includes Refs. [33–37,39–49].
[39] K. S. Novoselov, V. I. Fal'ko, L. Colombo, P. R. Gellert, M. G. Schwab, and K. Kim, A roadmap for graphene, Nature (London) **490**, 192 (2012).
[40] Z. Q. Li, E. A. Henriksen, Z. Jiang, Z. Hao, M. C. Martin, P. Kim, H. L. Stormer, and D. N. Basov, Dirac charge dynamics in graphene by infrared spectroscopy, Nat. Phys. **4**, 532 (2008).
[41] Z. Fei, A. S. Rodin, G. O. Andreev, W. Bao, A. S. McLeod, M. Wagner, L. M. Zhang, Z. Zhao, M. Thiemens, G. Dominguez *et al.*, Gate-tuning of graphene plasmons revealed by infrared nano-imaging, Nature (London) **487**, 82 (2012).
[42] Z. Fang, S. Thongrattanasiri, A. Schlather, Z. Liu, L. Ma, Y. Wang, P. M. Ajayan, P. Nordlander, N. J. Halas, and F. J. García de Abajo, Gated tunability and hybridization of localized plasmons in nanostructured graphene, ACS Nano **7**, 2388 (2013).
[43] Z. Fang, Y. Wang, A. E. Schlather, Z. Liu, P. M. Ajayan, F. J. García de Abajo, P. Nordlander, X. Zhu, and N. J. Halas, Active tunable absorption enhancement with graphene nanodisk arrays, Nano Lett. **14**, 299 (2014).
[44] A. Ishikawa and T. Tanaka, Plasmon hybridization in graphene metamaterials, Appl. Phys. Lett. **102**, 253110 (2013).
[45] A. D. Liao, J. Z. Wu, X. Wang, K. Tahy, D. Jena, H. Dai, and E. Pop, Thermally limited current carrying ability of graphene nanoribbons, Phys. Rev. Lett. **106**, 256801 (2011).
[46] Y. Li, H. Yan, D. B. Farmer, X. Meng, W. Zhu, R. M. Osgood, T. F. Heinz, and P. Avouris, Graphene plasmon enhanced vibrational sensing of surface-adsorbed layers, Nano Lett. **14**, 1573 (2014).
[47] C. A. Downing and G. Weick, Topological plasmons in dimerized chains of nanoparticles: Robustness against long-range quasistatic interactions and retardation effects, Eur. Phys. J. B **91**, 253 (2018).
[48] C. A. Downing, T. J. Sturges, G. Weick, M. Stobinska, and L. Martin-Moreno, Topological phases of polaritons in a cavity waveguide, Phys. Rev. Lett. **123**, 217401 (2019).
[49] I. Silveiro, J. M. P. Ortega, and F. J. García de Abajo, Plasmon wave function of graphene nanoribbons, New J. Phys. **17**, 083013 (2015).
[50] S.-X. Xia, D. Zhang, Z.-Z. Zheng, X. Zhai, H.-J. Li, J.-Q. Liu, L.-L. Wang, and S.-C. Wen, Topological plasmons in stacked graphene nanoribbons, Opt. Lett. **48**, 644 (2023).
[51] W. Song, W. Sun, C. Chen, Q. Song, S. Xiao, S. Zhu, and T. Li, Robust and broadband optical coupling by topological waveguide arrays, Laser Photonics Rev. **14**, 1900193 (2020).
[52] L. Lu, J. D. Joannopoulos, and M. Soljačić, Topological photonics, Nat. Photon. **8**, 821 (2014).
[53] T. Y. Abi-Salloum, Electromagnetically induced transparency and Autler-Townes splitting: Two similar but distinct phenomena in two categories of three-level atomic systems, Phys. Rev. A **81**, 053836 (2010).
[54] B. Peng, S. K. Ozdemir, W. Chen, F. Nori, and L. Yang, What is and what is not electromagnetically induced transparency in whispering-gallery microcavities, Nat. Commun. **5**, 5082 (2014).

Correction: Support information in the Acknowledgments was incomplete and has been fixed.